Archaeological and Anthropological Sciences
https://doi.org/10.1007/s12520-017-0578-2

ORIGINAL PAPER

Exploring ironmaking practices at Meroe, Sudan—a comparative analysis of archaeological and experimental data

Michael Charlton[1] · Jane Humphris[1]

Received: 16 August 2017 / Accepted: 27 November 2017

Abstract
Recent excavations of a Late to Post-Meroitic furnace workshop at Meroe, Sudan prompted questions concerning the use of some of its unusual design features and the nature of ironmaking practice. To begin addressing these questions, four iron smelting experiments were conducted in a purpose-built workshop modelled from the archaeological remains. Some of the goals of the campaign included identification and testing of potential ore and technical ceramic resources as well as the production of slag with characteristics that mirrored those of the archaeological deposits. The primary objective, however, was the further development of a model for Late to Post-Meroitic direct process iron production. Comparison of the microstructural and chemical characteristics of the archaeological and experimental ironmaking residues leads to a rejection of hypothesised ore sources adjacent to Meroe, support for hypothesised technical ceramic resource locations and a failure to replicate Late–Post-Meroitic smelting slag. However, the comparison also makes a strong contribution to the developing model of smelting practice at Meroe by emphasising the need to create more consistent redox conditions within the furnace, greater standardisation in preparing technical ceramics and the use of relatively lean ores (≈ 60 wt.% Fe).

Keywords Iron smelting · Experimental archaeology · X-ray microanalysis · Africa · Sudan · Kush · Meroe

Introduction

The production of iron, even at small scales, requires the complex coordination of social, technological and economic know-how. Ore must be prospected, mined, transported and prepared (usually roasting, crushing and sorting). Charcoal must be prepared by the slow burning of felled trees or branches, crushed to suitable size and similarly transported to the primary production site. These two main ingredients are then combined with air and flame within a furnace, which itself requires the accumulation and processing of materials such as stone and clay. The ironmasters, if successful, blend their accumulated resources and labour with knowledge and skill to yield a mass of iron and some quantity of residuum termed slag. Most of the iron metal, being the ironmaster's most valuable economic product, finds its way out of the workshop and into the hands of others as either raw material or finished artefacts. The slag along with any primary material losses are dumped in scatters or heaps that, in addition to remnant workshops, offer the only clues to past ironmaking behaviours. The hypotheses they generate, however, must be assessed through archaeologically constrained experimentation.

The Royal City of Meroe, now part of a UNESCO World Heritage listing (Archaeological Sites of the Island of Meroe), was once the capital of the Kingdom of Kush and the focus of Kushite political power between the third century BC and the fourth century AD (Humphris n.d.; Welsby 1996; Török 2015). The numerous large piles of ironmaking residues also mark the city as one of Africa's most impressive ancient iron production centres (see Humphris and Rehren 2014) or a summary of relevant literature. Meroe has at times been postulated as a focus for the diffusion of iron from the north throughout sub-Saharan Africa and as the recipient of ironmaking technology from Ethiopia to the south (Trigger 1969 and references therein). Ongoing archaeological research at Meroe (since 2012) so far includes intensive systematic investigation of seven slag heaps from the more than 30 mapped at ground level (not including the numerous slag deposits existing within the deep stratigraphy across parts of the site).

✉ Michael Charlton
m.charlton@ucl.ac.uk

[1] UCL Qatar, Doha, Qatar

Published online: 08 December 2017

Radiocarbon dating indicates over a thousand years of iron production (Humphris n.d.; Humphris and Scheibner 2017). The scale, intensity and continuity of production represented by such large quantities of slag are amongst the major research goals of the project.

One particular slag heap, Meroe Iron Slag 6 (MIS6), was excavated in 2014 after geophysical surveys indicated the presence of a potential furnace workshop (Fig. 1; Humphris and Carey 2016). The excavation exposed a floor displaying typical characteristics of Late Meroitic iron production workshops (Fig. 2; see Humphris n.d.; Shinnie and Kense 1982; Tylecote 1982) with a well-preserved furnace base at the eastern end. Radiocarbon dating indicates that many of the iron production residues found in association with the workshop date to Late Meroitic times, though the final use of the workshop took place in the early fifth century AD (see Humphris and Scheibner 2017 for details). The dates also indicate continual iron production into the Post-Meroitic period (Humphris and Scheibner 2017).

The MIS6 workshop was situated on the south side of the slag heap and was built into the remains of an earlier Meroitic structure. Prominent workshop features include a rectangular sunken workshop floor (about 30 cm lower than original ground level) with a shallow oval pit in the centre. The sunken floor measures approximately 2.5 × 4 m. A few centimetres of the lower portions of a single furnace with an internal diameter of 55 cm was preserved on the eastern end of the workshop. A second smithing feature was identified on the western end of the workshop. The overall plan of the workshop parallels those of similar date that were excavated in the 1970s (Shinnie and Kense 1982; Tylecote 1982).

The results of the MIS6 workshop excavation combined with those observed by Shinnie and Kense (1982) generated a rough blueprint for Late to Post-Meroitic furnace and workshop spaces that was amenable to empirical evaluation. The importance of experimental iron smelting as an investigative tool has been demonstrated repeatedly in both laboratory (Tylecote et al. 1971) and field (Crew 2000, 2013; Crew et al. 2012) settings. The fundamental role played by material production in economic systems mandates an accurate portrayal of its costs and benefits, a portraiture that can only be evaluated by controlled experiment.

In January 2015, a workshop modelled from the archaeological data was constructed at the Royal City of Meroe in order to run a series of experimental iron smelts that might provide scientific insights into the ancient ironmaking activities. Organised as part of a community engagement event (Humphris et al. n.d.a, b), four experiments were conducted within the reconstructed space that, in addition to creating a tangible experience for visitors (Fig. 3), were designed to illuminate the technological recipes followed by Late and Post-Meroitic ironmasters. Scientific goals included identifying furnace resources and preparation procedures; evaluating the function of the specialised 'furnace lining' found scattered on the site, exploring the design of the air intake mechanisms and developing a model of general furnace operation procedures—ore to fuel ratios, charging regime and management of the air supply. Modelling the quantities of iron and slag produced per smelt was also a key research agenda and essential for shedding light on the extinct Meroitic socioeconomy. These, of course, were ambitious goals that could not hope to be achieved in total after a few smelts constrained by time, logistics and cost.

Macroscopic observations from the smelts and the materials it generated are detailed in Humphris et al. (n.d.a, b) and summarised below. Table 1 summarises the experimental design and yields while the materials, organisation, recipe and product yields of the experiments are depicted in Fig. 4. As far as possible, the archaeological record was replicated including crushing ore to a 1–2-cm^3 size, attempting to use a similar charcoal (acacia type *Nilotica*) and attempting to replicate the technical ceramics (TC) using local materials. Despite these efforts, the production of slag equivalent to those of the archaeological record remained elusive in both expected quantities and character. The archaeological slag contained tap slag, ropey slag stringers and dense furnace slag. Except from a single run of tap slag, most of the experiments produced a viscous furnace slag with high porosity whose friable materials broke into sharp fragments.

Potential causes for the poor correspondence between the experiments and archaeology were suggested based on the observations at hand. Furnace temperature records indicated that MS1 failed to generate enough heat during the first 3 h of charging which led to poor yields. The failure of MS2 was variously blamed on the use of a low-quality ore, the high humidity of the day and a furnace that was too hot/too reducing during later stages of the smelt. MS3 produced a furnace slag with slightly lower viscosity, though low temperatures at the start of the smelt followed by high heat and reducing conditions at the end probably let to reduced yields and poor slag production. There was a sense, throughout the first three experiments, that the charge was reacting too strongly with the ceramic furnace wall, especially near the intersections of the wall with the tuyères. The use of a refractory lining in MS4 aimed to correct this problem but failed to cure in time for the smelt. The added moisture was suspected of preventing the build-up of sufficient heat and reducing conditions for bloom production and the development of a fluid slag. Through it all, there was a sense that the air supply system was also problematic, specifically the use of tuyères that plunged some 20–25 cm into the furnace from the internal wall and pot-bellows constructed with a shallow diaphragm and basal nozzle. Nonetheless, the experiments illuminated key features of Late–Post-Meroitic smelting practice including operational constraints within the workshop space and the accessibility of potential material resources.

Fig. 1 Map of Meroe and its slag heaps

Fig. 2 Final excavation photograph of the MIS6 workshop

The archaeometric examination of experimental resources and smelting products in direct comparison with those found in the archaeological record helps extend these insights by highlighting microscopic and chemical variation within and between groups defined by context and shedding light on fundamental recipe differences. In addition, explanations for experimental failures can be assessed against expected slag characteristics like the quantities and types of iron oxides present in the microstructure. Most importantly, the systematic comparison of experimental and archaeological samples, as presented here, provides the opportunity to check potential models of Late–Post-Meroitic smelting practices against reality and develop a deeper understanding of past technological choices and outputs. There may be many ways to smelt iron, even when following the constraints of the archaeological record, but any given furnace workshop followed a restricted set of these.

Fig. 3 Members of the local community observing an iron smelt in the experimental workshop during the smelting festival

Investigative methods

Sample selection and preparation

Materials from each smelting experiment were collected as completely as possible. Some compromises were made in the recovery process in order to accommodate the smelting festival schedule. Larger products, such as blooms, tuyère fragments and slag masses were bagged immediately while others were collected en masse in metal drums to cool and be sorted later by hand and magnet. This included material that was shovelled directly from the furnace. Care was taken not to sample material that became integrated with the sandy floors of the workshop as those contained were contaminated with small quantities of archaeological slag. Observations were not recorded, however, for slag that could not be dislodged from the furnace wall without damage or of volume changes to the furnace wall. These necessary compromises created bias in the recorded weights of the smelting products, but not the sampling of material for microscopic and chemical analysis.

Priority was given to slag during sampling because it provides the best single proxy for smelting recipes. Time limitations combined with the volume of materials being considered necessitated that a relatively small subsample be taken from the experimental residues. Specimens were selected to represent: (1) a cross-section of slag pulled from different locations within the furnace (those sampled during the experiment) and (2) slag with positive and neutral response when exposed to a typical hand magnet. A total of six slag specimens were sampled from MS1, five from MS2, seven from MS3 and six from MS4. These specimens are identifiable in the raw data by the '-S' suffix in the specimen name (Charlton and Humphris 2017). Approximately 5 kg of crushed roasted ore was collected from each homogenised batch to provide an analytical sample for each experiment. The analytical sample included five specimens from MS1 (1 doline + 4 purple), five from MS2, four from MS3 and four from MS4. These are identifiable in the raw data by the '-O' suffix in the specimen name (Charlton and Humphris 2017). A smaller sample TC was collected from the experiments since no change was made in the ceramic recipes across the campaign. The sample included three specimens from MS1, two from MS4 and one generic specimen removed from the furnace arch following MS4. These specimens are identifiable in the raw data by the '-T' suffix in the specimen name (Charlton and Humphris 2017).

Table 1 Summary of the design and yield performance of the January 2015 Meroe smelting experiments (see Humphris et al. n.d.a, b for more details)

Experiment	Ore type	Air supply	Ore:fuel (kg/charge)	Bloom (kg) (bloom/ore)	Slag (kg)	Part reduced ore (kg)	Observations
MS1 22 Jan 2015	50% doline; 50% purple	Natural draft (16 charges). Forced draft (25 charges; 60–120 strokes/min)	41 × 1:1	4.325 (0.105)	19	4	Viscous slag—no flows
MS2 25 Jan 2015	Purple	Natural draft (6 charges). Forced draft (24 charges; 60–130 strokes/min)	30 × 1:1	0 (NA)	11	9	Viscous slag—no flows. Small amounts of cast iron (not quantified)
MS3 26 Jan 2015	Oolitic	Natural draft (10 charges). Forced draft (10 charges; 60–110 strokes/min)	20 × 1.5:1	1.5 (0.05)	15	4	Internal slag flows
MS4 28 Jan 2015	Oolitic	Natural draft (2 h). Forced draft (25 charges; 60–110 strokes/min)	4 × 2.5:3; 4 × 3.5:3; 2 × 5:3	0 (NA)	12	4.5	Pre-charged with ore and charcoal. Furnace lining added but not cured prior to smelt. One flow of tap slag

There is a fundamental difference in scale when sampling the products of a single experimental smelt, compared with sampling the products of numerous smelts accumulated in heterogeneous slag heap over a number of years or decades in the archaeological record (Humphris and Carey 2016). To mitigate this, the archaeological smelting residues analysed here were sampled from the fill of the furnace base (collected as a bulk sample during excavation) and assumed to contain the products of the last firing of the furnace (Fig. 5). Contamination from the overlying burden of the slag heap, however, cannot be ruled out. The sandy matrix of the furnace fill was sieved through 1 mm mesh and larger materials sorted into stone, slag, ore and TC based on macroscopic characteristics (especially colour, texture, density, magnetism, inclusion presence and porosity). Most materials were small and fragmented, although some slag was large enough to identify as internal furnace flows, or prills and furnace slag. A sample of these materials was selected for analysis including 15 slag, 7 ore and 5 TC specimens. Again, more emphasis was placed on the sampling of slag than other materials and reflected the possibility that macroscopic identification might be in error when dealing with specimens of small size.

Subsamples of experimental and archaeological materials were microscopically and chemically characterised at the UCL-Qatar Archaeological Materials Science Laboratories in Doha. These specimens were sectioned, cleaned and mounted in blocks of epoxy resin, and then polished using standard metallographic techniques to a finish of 1 μm. All

Fig. 4 Components of the experimental smelting recipes and their results. **a** roasted and crushed ore; **b** acacia charcoal; **c** furnace construction materials; **d** furnace design; **e** tuyères; **f** bellows; **g** furnace operation by the team; **h** forged iron billet; **i** slag

Fig. 5 MIS6 furnace section during excavation showing the base of the furnace from which the bulk sample for analysis was collected

specimens were examined via optical microscopy and then coated with a thin film of carbon for scanning electron microscopy (SEM) and X-ray microanalysis via energy-dispersive spectroscopy (EDS).

Optical microscopy

Polished specimens were examined under reflected light with a Leica DM 2500P at magnifications of ×50, ×100 and ×200. Phases and their morphologies, along with any observed anomalies, were noted, and reference images were taken for most specimens. Secondary material characterisation was made based on the microscopically identified features and applied to each specimen prior to chemical analysis (see Charlton and Humphris 2017 for images and material identifications).

Scanning electron microscopy and X-ray microanalysis

Polished carbon-coated specimens were further examined with a JEOL JSM 6610 low vacuum SEM equipped with an Oxford Instruments X-Max ^{N}50 energy dispersive spectrometer. Images were captured with backscattered electrons (BSE) to observe phase differences and element compositional analyses conducted for each. X-ray spectra were acquired, interrogated and quantified using Oxford Instruments *Aztec 3.1*. Spectra were optimised using a cobalt standard and acquisition parameters were kept constant (working distance = 10 mm; accelerating voltage = 20 kV; process time = 5; deadtime ≈ 40%). All EDS analyses were conducted as area scans at magnifications of ×200, resulting in analysed areas of 0.28 mm^2. A total of five scans were made for each specimen. The areas were chosen systematically to represent the average microstructure (and chemistry) of the sample across its entire area. The size of each area depended on the heterogeneity of each specimen; an even size distribution if the specimen had a homogeneous microstructure or a variable size distribution if clear differences were observed. The aim was to give proportional coverage to all microstructural features and provide an accurate estimate of the specimen's bulk chemistry. This step is important since many smelting residues, and especially slag, are often heterogeneous. Peak identifications were made manually in order to optimise each fitted spectrum to its empirical spectrum and identify anomalies created by the pulse pile up correction algorithm. SEM images, raw data and assessments of inter-specimen variability can be found in Charlton and Humphris (2017).

Data quality

The results of small surface area analyses using a beam technique are subject to analyst biases. Their reliability can only be evaluated quantitatively by direct comparison of homogenised specimens through true bulk techniques like X-ray fluorescence or inductively coupled plasma spectroscopy. The relative reliability of the technique, however, can be assessed by the ability to recognise discrete groups of materials defined a priori by context or experiment.

Three certified reference materials (CRM) were analysed as part of most analytical sessions to ensure stable instrument performance and provide a means of assessing the precision and accuracy of quantified results. The US Geological Survey CRM basalts BCR-2G (Plumlee 1998a), BIR-1G (Smith 1998) and BHVO-2G (Plumlee 1998b) were selected for this purpose. Results deviated from the recommended values and from one another due to variations in beam current and minor differences in focusing. Normalisation across all identified elements led to general increases in accuracies and precision for most elements with recommended values greater than 0.1 wt.% (Tables 2, 3 and 4). Low values of P and Mn are notable exceptions, creating less precise, but, in general, more accurate values. Results of all CRM analyses are reported in Charlton and Humphris (2017).

A decision was made to report results as elements rather than oxides—the latter being the more common approach in the literature. More than a preference, the decision is based on the fact that ED spectra identify elements, not compounds. Oxygen is amongst those elements and may be measured more precisely than calculating its presence by stoichiometry. This is particularly true when oxides of a given element, like Fe, may vary between the materials one wishes to compare. One can always calculate stoichiometry using the elemental data but may not be able to back transform to element weight per cent with the same confidence. More important is that phase structure and oxide choice tend to agree such that analytical totals approach 100 wt.%.

There are three main reasons why such totals may not be approached in any given case. First, beam currents may vary

Table 2 Recommended, mean and normalized mean values for SEM-EDS analyses of BCR-2G

BCR-2G	O	Na	Mg	Al	Si	P	K	Ca	Ti	V	Mn	Fetot	Zn	Sr	Zr	Mo	Ba	Ce
Recommended																		
wt.%	44.96	2.34	2.16	7.14	25.30	0.15	1.49	5.09	1.35	0.04	0.15	9.66	0.01	0.03	0.02	0.02	0.07	0.01
±		0.08	0.03	0.10	0.40	0.01	0.04	0.08	0.03	0.00	0.01	0.15	0.00	0.00	0.00	0.00	0.00	0.00
Analyzed n = 13																		
ȳ (wt.%)	46.04	2.48	2.28	7.56	26.60	0.16	1.59	5.34	1.45	0.06	0.16	10.05	0.00	0.04	0.04	0.02	0.12	0.02
s (wt.%)	0.89	0.06	0.05	0.13	0.41	0.01	0.02	0.09	0.03	0.02	0.02	0.13	0.01	0.08	0.04	0.02	0.04	0.03
% RSD*	1.97	2.44	2.10	1.76	1.59	8.65	1.37	1.65	2.46	23.76	13.08	1.30	367.49	196.18	116.39	118.94	36.67	189.48
E (wt.%)	1.08	0.14	0.12	0.42	1.30	0.01	0.10	0.25	0.10	0.02	0.01	0.39	− 0.01	0.01	0.02	− 0.01	0.06	0.01
% E	2.39	5.85	5.52	5.91	5.14	4.10	6.76	4.94	7.35	55.33	7.79	4.00	− 81.83	17.83	100.49	− 25.56	82.45	219.30
Normalized (n = 13)																		
ȳ (wt.%)	44.26	2.38	2.19	7.27	25.57	0.15	1.53	5.14	1.39	0.06	0.16	9.66	0.00	0.04	0.04	0.02	0.12	0.02
s (wt.%)	0.21	0.03	0.02	0.03	0.07	0.01	0.02	0.05	0.03	0.01	0.02	0.11	0.01	0.08	0.04	0.02	0.04	0.03
% RSD*	0.48	1.49	0.87	0.47	0.29	*8.93*	1.17	0.93	2.13	22.91	12.76	1.14	367.49	196.75	*115.77*	119.60	*37.01*	*189.81*
E (wt.%)	− 0.70	0.04	0.03	0.13	0.27	0.00	0.04	0.05	0.04	0.02	0.01	0.00	− 0.01	0.00	0.02	−0.01	0.05	0.01
% E (%)	− apxnver1.56	1.77	1.45	1.83	1.08	0.12	2.66	0.90	3.22	49.13	3.61	0.00	− 82.53	*13.40*	91.97	− 28.42	*75.79*	205.06

Standard deviations (S), corrected relative standard deviations (% RSD*), absolute errors (E) and relative errors (% E) are provided for comparison of analysed and normalized values. Values set in italics indicate worse performance post-normalization

and influence the calculated totals. Totals amongst the CRMs, for example, sometimes reached 111 wt.% and could be corrected with normalisation as noted above. Second, low totals will occur when voids are present. This is only partially correctable by normalisation and reduces accuracy to an unknown level. Where porosity is similar between specimens, their relative chemical variation will be maintained. Caution, however, is warranted when levels of porosity are dissimilar, as in the case of samples from different materials. A third reason that totals might deviate from 100 wt.% is a poor analysis caused by instrument failure, improper instrument configuration or exceptionally bad sample preparation. An examination of the data created in this study indicates that deviations are caused by changes in beam current and levels of porosity. No individual specimens were removed from consideration.

Material characterisation

Iron production generates a broad range of residual materials, many of which have blurred definitions. Categories used here include: ore—ferruginous stone comprised of goethite and silica grains of varying size and structure; part-reduced ore (PRO)—ore showing increasing quantities of ferrous oxide skins as well as reactions with alumina and silica that result in irregularly structured hercynite and fayalite crystals; smelting slag—a once molten or semi-molten ferrosilicate comprised mainly of fayalite, wüstite, glass and possibly hercynite; smithing slag—smelting slag that has reacted with ceramics from the smithing hearth, additional quantities of fuel ash and hammer scale; bloom slag—slag that adheres to the bloom and often contains high levels of silica and lime relative to most other smelting slag; fuel ash slag—vitreous

Table 3 Recommended, mean and normalized mean values for SEM-EDS analyses of BIR-1G

BIR-1G	O	Na	Mg	Al	Si	P	K	Ca	Ti	V	Cr	Mn	Fe	Co	Ni	Cu	Zn	Sr
Reference																		
wt.%	43.90	1.35	5.85	8.20	22.42	0.01	0.02	9.51	0.58	0.03	0.04	0.14	7.90	0.01	0.02	0.01	0.01	0.01
±		0.03	0.05	0.08	0.09	0.00	0.00	0.09	0.01	0.00	0.00	0.00	0.08	0.00	0.00	0.00	0.00	0.00
Analyzed (n = 13)																		
ȳ (wt.%)	46.07	1.41	6.18	8.75	23.56	0.00	0.03	10.04	0.63	0.04	0.05	0.15	8.39	0.06	0.02	0.04	0.01	0.05
s (wt.%)	1.13	0.05	0.15	0.20	0.53	0.00	0.01	0.22	0.02	0.01	0.02	0.02	0.15	0.03	0.02	0.03	0.02	0.10
% RSD*	2.50	3.56	2.45	2.31	2.30	159.13	44.75	2.23	2.77	34.50	44.55	12.47	1.77	52.79	104.11	73.51	227.46	194.04
E (wt.%)	2.17	0.06	0.33	0.54	1.14	− 0.01	0.00	0.54	0.05	0.01	0.01	0.01	0.49	0.05	0.01	0.03	0.00	0.04
% E	4.93	4.26	5.70	6.63	5.08	− 66.43	8.11	5.63	8.96	29.03	22.66	8.41	6.17	1039.05	31.22	232.31	31.87	389.51
Normalized (n = 13)																		
ȳ (wt.%)	43.68	1.33	5.86	8.29	22.33	0.00	0.03	9.52	0.59	0.04	0.04	0.14	7.96	0.06	0.02	0.04	0.01	0.05
s (wt.%)	0.19	0.03	0.04	0.04	0.04	0.00	0.01	0.05	0.01	0.01	0.02	0.02	0.10	0.03	0.02	0.03	0.02	0.10
% RSD*	0.44	2.24	0.61	0.53	0.20	*159.16*	*45.10*	0.59	2.44	*35.09*	43.91	*12.99*	1.23	*52.82*	*104.47*	73.41	227.44	194.01
E (wt.%)	− 0.23	− 0.02	0.01	0.09	− 0.08	− 0.01	0.00	0.01	0.02	0.01	0.01	0.00	0.05	0.05	0.00	0.03	0.00	0.04
% E	− 0.52	− 1.16	0.22	1.09	− 0.37	− *67.73*	2.66	0.15	3.32	22.60	16.21	2.85	0.68	981.10	24.58	215.28	22.69	366.15

Standard deviations (S), corrected relative standard deviations (% RSD*), absolute errors (E) and relative errors (% E) are provided for comparison of analysed and normalized values. Values set in italics indicate worse performance post-normalization

Table 4 Recommended, mean and normalized mean values for SEM-EDS analyses of BHVO-2G

BHVO-2G	O	Na	Mg	Al	Si	P	K	Ca	Ti	V	Cr	Mn	Fetot	Ni	Cu	Zn	Sr	Zr	Ba
Reference																			
wt.%	44.27	1.64	4.36	7.16	23.30	0.12	0.43	8.17	1.63	0.03	0.03	0.13	8.63	0.01	0.01	0.01	0.04	0.02	0.01
±		0.06	0.07	0.08	0.30	0.01	0.01	0.12	0.20	0.00	0.00	0.00	0.14	0.00	0.00	0.00	0.00	0.00	0.00
Analyzed (n = 13)																			
ȳ (wt.%)	46.34	1.74	4.67	7.66	24.71	0.13	0.46	8.60	1.79	0.04	0.02	0.14	8.98	0.01	0.01	0.01	0.03	0.03	0.04
s (wt.%)	1.25	0.05	0.14	0.20	0.61	0.01	0.02	0.21	0.06	0.02	0.01	0.02	0.22	0.02	0.01	0.02	0.10	0.03	0.05
% RSD*	2.74	2.65	3.05	2.69	2.52	9.16	4.12	2.46	3.15	40.73	73.25	12.13	2.55	147.96	118.85	148.86	367.49	111.86	110.47
E (wt.%)	2.07	0.10	0.31	0.50	1.41	0.01	0.03	0.43	0.16	0.01	− 0.01	0.01	0.35	0.00	0.00	0.00	− 0.01	0.01	0.03
% E (%)	4.68	6.00	7.20	6.93	6.06	4.49	7.33	5.26	9.72	33.46	− 31.32	7.93	4.08	3.43	− 15.20	34.43	− 30.79	56.53	225.44
Normalized (n = 13)																			
ȳ (wt.%)	43.96	1.65	4.43	7.26	23.44	0.12	0.44	8.16	1.70	0.04	0.02	0.13	8.52	0.01	0.01	0.01	0.03	0.03	0.04
s (wt.%)	0.17	0.02	0.03	0.03	0.04	0.01	0.01	0.04	0.03	0.02	0.01	0.02	0.07	0.02	0.01	0.02	0.09	0.03	0.04
% RSD*	0.40	1.25	0.72	0.41	0.17	8.73	3.40	0.53	1.58	40.79	*73.54*	*13.60*	0.83	*149.42*	*120.05*	*149.62*	*367.49*	*110.59*	109.84
E (wt.%)	− 0.31	0.01	0.07	0.10	0.14	0.00	0.01	− 0.01	0.07	0.01	− 0.01	0.00	− 0.11	0.00	0.00	0.00	− 0.01	0.01	0.03
% E	− 0.70	0.57	1.69	1.44	0.62	− 0.88	1.83	− 0.14	4.09	26.41	− *34.48*	2.57	− 1.26	− 0.64	− 19.33	28.73	− 32.64	47.34	208.96

Standard deviations (s), corrected relative standard deviations (% RSD*), absolute errors (E) and relative errors (% E) are provided for comparison of analysed and normalized values. Values set in italics indicate worse performance post-normalization

material with high lime, potash and magnesia concentrations formed from the reactions of fuel ash and TC, ceramic rich slag—vitreous slag with high alumina and silica contents that forms from the reaction of TC; TC—remanent fragments of furnace wall and tuyères; and gromp—fused bits of slag and unconsolidated iron that often forms on top of blooms. Broad categories like ore, slag and TC display distinct macroscopic and microscopic characteristics that make them easy to sort. Small fragments of slag and TC collected from the archaeological furnace fill could be identified based the presence of fayalite and silica grains, respectively. Distinguishing ore samples from PRO was more challenging.

All ore samples collected from archaeological materials were assumed to be reacted to varying degrees, some of which could be expected to be closer to slag in chemical composition and depleted of Fe. Ore fragment size was approximately 1–2 cm^3, the same as used in the experiments. The presence of ooids was the only reliable microscopic identifier but could not be trusted to identify all ore samples. This problem was mitigated by implementing a group identification procedure involving principal component analysis (PCA) and hierarchical cluster analysis (HCA). Employing functions from the R base package (R Core Team 2017), all specimens were subjected to standard PCA (following the terminology of (Baxter and Freestone 2003). That is, a PCA was applied to the standardised (z-score) values of all elements above the 0.1 wt.% for the materials under consideration. This is also equivalent to running the PCA on the correlation matrix. The PC scores were grouped using average-linkage HCA. Those specimens identified through microscopy as PRO were chemically distinct from slag and TC. The PCA and HCA procedures were repeated for the PRO specimens, and the group that contained the highest Fe concentrations was subsequently assigned to the 'ore' chemical group. All procedures and R code are provided in Charlton and Humphris (2017).

Similarly, some slag specimens contain fuel ash or ceramic enrichment that goes unnoticed in microscopic examination. These enrichments can be detected chemically, following the same procedures outlined above. The identification of discrete slag groups whose members are enriched in Al, Si and Ti indicate stronger TC influence, while those rich in Ca, K and Mg are indicative of stronger fuel ash influence (see Charlton et al. 2010). Such enrichments are identified by the strong positive correlation of the relevant element loadings. Outlying groups of slag with either of these enrichments were removed from consideration in order to make reasonable material comparisons. It is worth noting that structurally distinct groups include members derived from multiple experiments. The iterative procedure for removing outliers was repeated until no distinct outliers could be detected from any single experimental or archaeological group. Charlton and Humphris (2017) provide a step-by-step account of the entire procedure with supporting graphs.

Resource and recipe hypotheses

Direct comparisons were made between experimental and archaeological ores, TC and slag. Nominal-scale microstructural variation was noted, and the chemistry of all samples was evaluated with PCA. Affinities between microstructural and chemical groups (defined by context or experiment number) indicate similarities in exploitation (in the case of ores and TC) and use (in the case of slag). Given the small sample sizes and lack of repeated trials, the statistical significance of such similarities and differences was not evaluated.

Reduction efficiency and resource costs

Ironmaking recipes are compared in three ways. The first comparison relies on plotting slag chemistry within the $FeO–SiO_2–Al_2O_3$ ternary-phase diagram. This equilibrium diagram is an effective thermochemical model for most ferrosilicate slags. Though representing an ideal system somewhat different from the non-equilibrium conditions of bloomery furnaces, it nonetheless provides a means of comparing smelting recipes and making inferences about the technological choices of the smelters (Rehren et al. 2007; Charlton et al. 2010). The second involves calculation of the reducible iron index (RII; see Charlton et al. 2010) which serves as a proxy for redox conditions within a bloomery furnace. The validity of RII requires that any element or oxide concentrations in the slag influenced from non-ore parental materials must be estimated and removed prior to comparison. This is achieved by means of mass balance calculations, the third method. Mass balances estimate the resource proportions required by the system to generate a slag with a specified chemistry, as well as the amount of iron produced per unit of slag.

Both the ternary phase diagram and RII calculation require a conversion of elements into oxides. The procedures and multipliers used are provided in Charlton and Humphris (2017). In both cases, MnO is added to FeO because the two are common ore constituents and MnO behaves similarly to FeO in the smelting context (Mn is only one proton less than Fe). Other oxides, such as CaO and MgO, while often behaving in a similar fashion to FeO, are less prevalent in ores and are more likely derived from fuel ash. They should not be included unless a strong case can be made for them deriving primarily from the ore.

Results

Ore

A key goal for the experimental campaign was the identification of reasonable ore resources. Ores were grouped into three types based on macroscopic inspection by the lead smelter. These included, in order of use, doline—a fine-grained oolitic ironstone associated with filled-sinkholes (dolines), purple—a soft and variable ironstone crust found in the hills behind the Meroe Pyramids and oolitic—an ironstone with a recognisable spheroidal texture also acquired in the hills behind the pyramids. Representative backscattered electron micrographs of the three ore varieties are shown in Fig. 6 in comparison with similar samples analysed from the MIS6 furnace.

Clear differences are revealed in the microstructures of the experimental ores (Fig. 6a–c), and the potential ores recovered from the archaeological workshop (Fig. 6d–f). The doline and oolitic ores are most similar in structure, containing a series of Fe-rich ooids of varying size. The so-called oolitic ore is more weathered and contains higher numbers of vesicles within its matrix. The microstructure of the purple ores contains a network of Fe-rich phases and large voids, giving them the appearance of trabecular bone or a mass of microfossils. The potential archaeological ores contain a series of round structures that resemble the ooids of the experimental ores, but with a more prominent radial structure and less obvious concentric rings. Other examples are more amorphous in structure and the pattern of vesicles resembles that of the purple ores.

Systematic differences are also observed in ore chemistry (Table 5), with variation in all elements measured above 0.1 wt.%. PCA biplots of the first three PC axes reveal the patterns in ore chemistry and highlight the greater similarity between the potential archaeological ores and the purple ores used in experiments MS1 and MS2. The doline and oolitic ores are richer in Fe, with lower concentrations of Al and Si. The doline ores have higher concentrations of P and lower Co relative to the oolitic ores. The purple ore is characterised by higher Al concentrations relative to those found within samples taken from MIS6 (Fig. 7).

Though the doline and oolitic ores seem more appropriate for effective bloomery smelting based on their relative richness in Fe compared with refractory elements, it is clear that they are not related to the archaeology of MIS6. These ores do share similar ooid grain sizes with those from the MIS6 furnace, but the more fractured character of the latter may have led to greater penetration of reducing gasses. This might have made the archaeological ores more reducible despite their relative leanness in Fe.

Technical ceramics

Little difference is observed between the experimental and archaeological TC microstructures (Fig. 8). This most likely reflects the use of the same or similar local resources, including Nile clay and surface sand. The only obvious microscopic difference between the two sample sets is the inclusion of slag in the temper of the archaeological ceramics (Fig. 9). Whether this addition is intentional or incidental cannot be determined

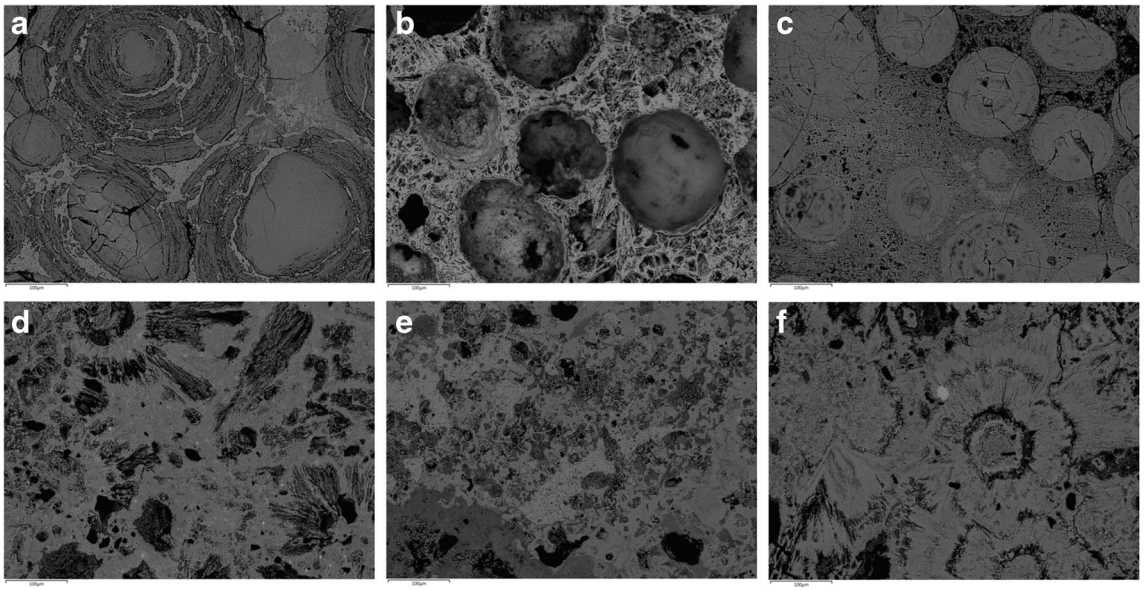

Fig. 6 BSE images of select ore specimens derived from the Meroe smelting experiments and the MIS6 furnace fill. **a** MS1-doline-3_area b; **b** MS2-purple-15-3_area c; **c** MS3-oolitic-1_area b; **d** MIS6-FW-224-1-O_area b; **e** MIS6-FW-224-3-O_area e; **f** MIS6-FW-6-O_area e. The full set of SEM images is available in Charlton and Humphris (2017)

(see Ting and Humphris 2017) for a more detailed consideration of TC produced at Meroe.

The experimental and archaeological TC samples are also chemically similar as seen in Table 6 and Fig. 10. The archaeological ceramics tend to be richer in Fe and Mn, probably reflecting a contribution from the slag temper. A second difference is that the archaeological ceramics have a more consistent chemistry. These findings are in agreement with the microscopic observations and suggest that the resources acquired for the experiments generally match those used by Late Meroitic furnace builders. The modern production, however, failed to replicate the precise recipe and skill of the ancients.

Slag

Investigations of the slag reveal high levels of microstructural diversity both within and between experiments and lower levels of variability within the archaeological slags. Figure 11 shows representative micrographs from each experiment and MIS6 (ordered MS1 through MS4 by row) with the bottom row showing MIS6. The experimental slag contains phases common to primary iron smelting slag, such as fayalite (Fe_2SiO_4), wüstite (FeO), hercynite ($FeAl_2O_4$) and glass. However, it also contains magnetite (Fe_3O_4)—a phase more often found in slag produced under more oxidising conditions (grey phase in Fig. 11a, d, i and l). Here, the presence of magnetite may also be indicative of ore particles that failed to reduce completely. The range of structures indicates formations in variable thermal and redox furnace environments. This observation is consistent with the character of the smelts as documented by the operation log and thermal profiles (Humphris et al. n.d.a, b). The archaeological slag, by contrast, is relatively lean and only contains fayalite, glass, some hercynite and small concentrations of wüstite. From the overall consistency and visibly low levels of wüstite (and other free iron oxides) in the MIS6 slag microstructure, it is

Table 5 Chemical summary of experimental and archaeological ore types for element concentrations greater than or equal to 0.1 wt.%

Type	wt.%	Na	Mg	Al	Si	P	Cl	K	Ca	Ti	Mn	Fe	Co	Sr	Ba
MIS6 (n = 6)	ȳ	0.29	0.26	1.99	6.23	0.50	0.30	0.18	0.65	0.34	1.21	57.36	0.26	0.06	0.05
	s	0.13	0.10	0.66	2.39	0.07	0.09	0.14	0.45	0.20	0.83	5.17	0.04	0.04	0.06
Doline (n = 3)	ȳ	0.07	0.06	1.43	0.97	0.62	0.05	0.01	0.14	0.05	0.31	64.94	0.30	0.07	0.05
	s	0.09	0.01	0.38	0.60	0.07	0.04	0.01	0.02	0.05	0.14	3.85	0.02	0.04	0.04
Purple (n = 5)	ȳ	0.10	0.02	3.82	4.35	0.35	0.27	0.04	0.17	0.19	1.22	60.92	0.30	0.07	0.11
	s	0.05	0.00	0.63	0.37	0.06	0.15	0.01	0.02	0.08	0.35	1.34	0.03	0.05	0.05
Oolitic (n = 8)	ȳ	0.04	0.24	1.43	1.75	0.51	0.15	0.15	0.20	0.04	0.64	68.88	0.34	0.10	0.02
	s	0.02	0.32	0.46	0.65	0.12	0.08	0.39	0.11	0.01	0.11	4.50	0.05	0.02	0.02

Means and standard deviations are calculated from normalized raw data found in Charlton and Humphris (2017)

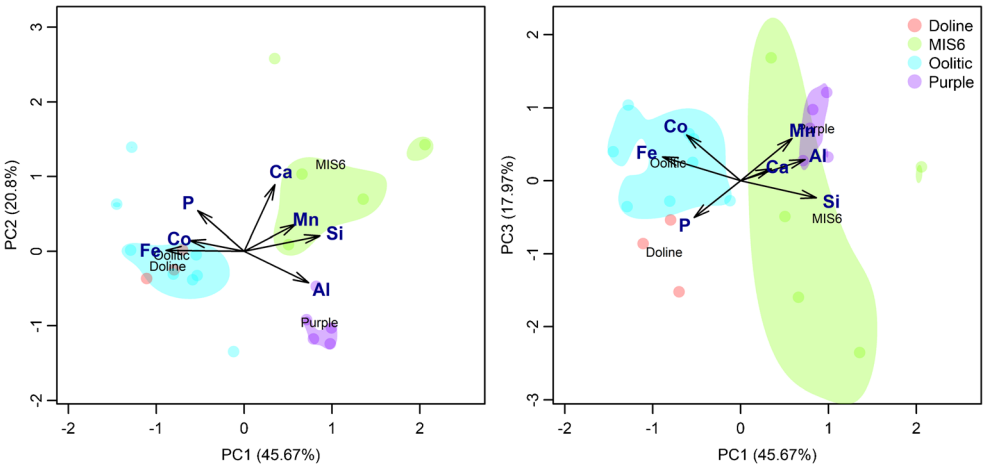

Fig. 7 PCA biplots of experimental and archaeological ore chemistry. Specimens include samples of roasted ore collected and processed for the Meroe bloomery experiments as well as samples excavated from the MIS6 furnace fill. Ore names are plotted at the centres of their projected distributions

hypothesised that the Meroitic ironmasters were effective in achieving high reduction efficiency through skilful replication of distinct recipes and smelting practices. MS2 and MS3 are the only experimental smelts to yield slag specimens with microstructures similar to the MIS6 furnace slag, perhaps reflecting higher redox conditions during particular times of the smelt (see Humphris et al. n.d.a, b).

Slag chemistry reveals extensive diversity between all smelts and the archaeology (Table 7). This reflects both the use of different ores and variation in furnace operation. A PCA of the slag chemistry is able to discriminate each group with little error (Fig. 12). The model proposed by (Charlton et al. 2013) can be invoked to generate hypotheses that account for the observed chemical differences based on variation in parent material contributions (Table 8) as specified strong positive correlations between element loadings.

The plot of PC1 vs. PC2 (Fig. 12, left) shows MIS6 to be discriminated by strong positive correlations of Si, Ti, Mn and Ba. These correlations can be estimated by the acute angle and similarities in magnitude of the loading vectors. The model indicates that this separation is due to chemical constraints imposed by ore differences and/or TC enrichment. MS1 slag is loosely discriminated by strong correlations of Na, Mg, Ca and P which the model indicates is a function of constraints imposed by differences in ore and/or fuel ash. The plot of PC1 vs. PC3 (Fig. 12, right) shows that MS3 and MS4 slag is

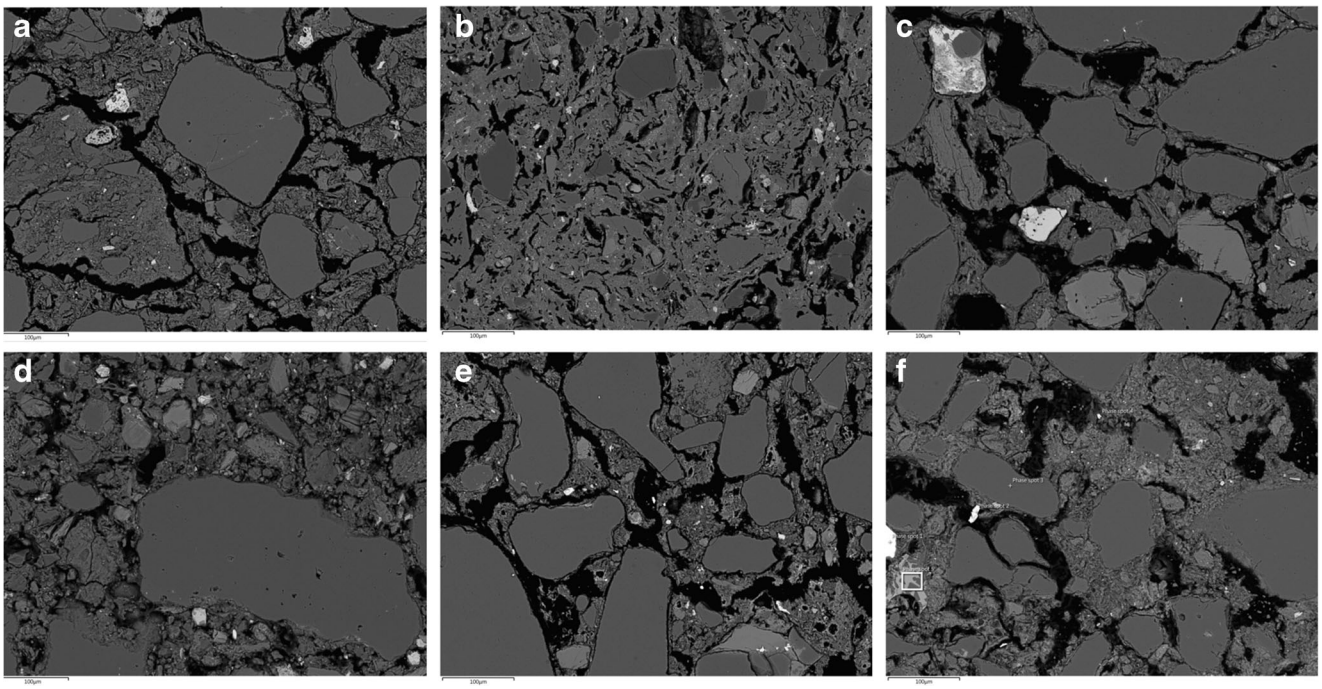

Fig. 8 BSE images of select technical ceramic specimens derived from the Meroe smelting experiments and the MIS6 furnace fill. **a** MS1-1-T_Area D; **b** MS1-2-T_Area B; **c** MS1-3-T_Area D; **d** MS4-2-T _Area B; **e** MIS6-FW-224-2-T_Area E; **f** MIS6-FW-224-3-T_Area A. See Charlton and Humphris (2017) for all SEM images collected in this study

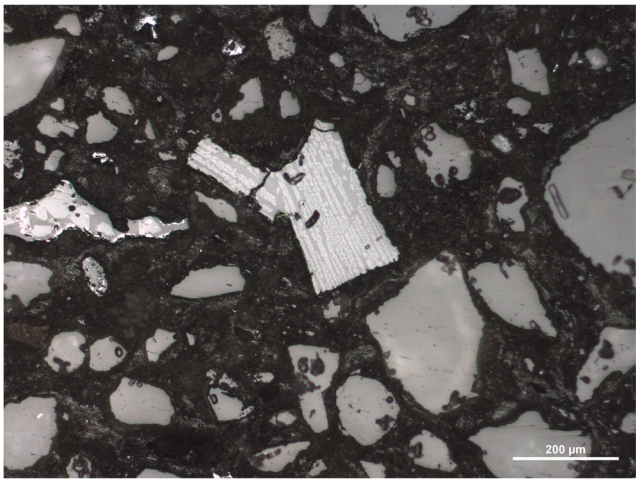

Fig. 9 Photomicrograph of slag temper (centre) in a technical ceramic specimen from MIS6 furnace fill (MIS6-FW-224-T). See Charlton and Humphris (2017) for all optical micrographs collected in this study

separated by the strong positive correlation of Fe and Co, indicating an ore difference. MS2 and MS4, however, are not well explained.

The autocorrelation of Fe and Si in ironmaking slags presents a limitation to this model. These elements are always negatively correlated and, in addition to being related to parent material chemistry, are also influenced by furnace redox conditions. The first PC axis can, therefore, also be interpreted as a ratio of Fe to Si. The discrimination of MIS6 slag may also be explained as the result of a more reducing furnace environment relative to the experimental slags. A second PCA of slag subcompositional variables was run to remove the confounding effects of Fe and Si. Figure 13 shows biplots of the first few PC axes of this analysis and adds greater clarity to the chemical constraints influencing the different production contexts. The strong positive correlations between Ba, Mn and Ti again indicate that the MIS6 slag was produced from a different ore. MS1 is again hypothesised to derive from a different ore and/or to be enriched by fuel ash. MS2 and MS3 slag show greater overlap and are discriminated by high positive correlations between Co and Al, reflecting an ore difference and their similarity in localised geochemical contexts. By comparison with the previous PCA of slag, the MS2 slag is hypothesised to be produced in a more reducing furnace environment than that of MS3, or having used an ore that was less rich in Fe. Both are true based on ore analyses (see Table 5) and smelt descriptions (see Table 1 above and Humphris et al. n.d.a, b). Slag from MS4 seems to be best separated by higher correlations of K and P, though it used the same ore as MS3. The best hypothesis to account for this surprising result is that MS4 slag incorporated greater quantities of fuel ash. The unique experimental design and complications of MS4 (i.e. the addition of a lining and the layered charges fits this explanation see Table 1 and Humphris et al. n.d.a, b). The slag, what little was produced, was allowed to sit in a relatively cool bed of charcoal in which it could dissolve additional quantities of fuel ash.

While it is clear that none of the ores used in the experiments match those used by the Meroitic smelters responsible for MIS6, the question still remains as to whether or not the archaeological material represents a stronger reducing environment or the use of a leaner ore. That is, despite ore differences, were the furnaces operated in a fundamentally different way? The hypothesis that furnace operation is different can be evaluated with the $FeO–SiO_2–Al_2O_3$ phase diagram, RIIs and mass balance calculations via Crew's (2000) method. As noted above, the validity of the second model depends on the results and accuracy of the third. Indeed, if reduction efficiency is to be evaluated on a ternary model, the same requirement holds. This requirement is not achievable, however, given the unknown error differences between SEM analyses of slag and TC required to formulate mass balances.

A partial way forward is provided by the fact that the MIS6 ores are similar in richness to the purple ore used in MS2, and

Table 6 Chemical summary of experimental and archaeological technical ceramics for element concentrations greater than or equal to 0.1 wt. %

Context	wt.%	Na	Mg	Al	Si	P	Cl	K	Ca	Ti	Mn	Fe
MIS6-FW224 (n = 5)	ȳ	0.47	0.68	3.58	37.27	0.06	0.51	0.79	1.57	0.41	0.20	5.48
	s	0.18	0.15	0.99	2.52	0.03	0.15	0.20	0.61	0.24	0.19	2.65
MIS6-FW224 (outlier)		1.01	0.94	4.40	26.53	0.10	0.75	1.37	7.11	0.41	0.25	5.10
MSarch (n = 1)		0.38	0.72	2.53	34.84	0.44	0.03	2.91	3.95	0.41	0.18	6.74
MS1 (n = 3)	ȳ	0.79	0.87	7.32	34.64	0.08	0.27	1.76	1.46	0.75	0.07	4.16
	s	0.84	0.72	3.74	6.48	0.09	0.05	1.64	1.11	0.25	0.05	2.95
MS4 (n = 2)	ȳ	0.33	1.15	7.11	32.99	0.10	0.24	0.50	2.77	0.70	0.06	3.71
	s	0.22	0.33	2.91	2.08	0.01	0.04	0.20	1.00	0.04	0.07	2.10
MS1 + MS4 (n = 5)	ȳ	0.60	0.98	7.24	33.98	0.09	0.26	1.26	1.99	0.73	0.06	3.98
	s	0.65	0.55	3.02	4.78	0.06	0.04	1.35	1.17	0.18	0.05	2.35

Means and standard deviations are calculated from normalized raw data found in Charlton and Humphris (2017)

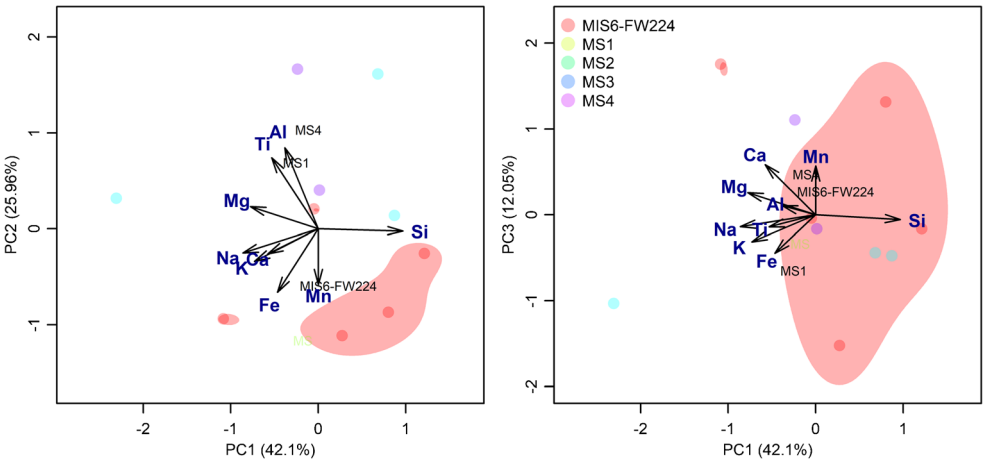

Fig. 10 PCA biplots of experimental and archaeological technical ceramic chemistry. Specimens include samples collected from the Meroe bloomery experiments as well as samples excavated from the MIS6 furnace. Technical ceramic context names are plotted at the centres of their projected distributions

there is no fundamental difference in other recipe ingredients (TC and charcoal) nor does the evidence indicate a difference in the fuel ash influence which might occur due to different charcoal types or blowing rate. Comparisons between these two samples can therefore illuminate ordinal-scale differences in redox conditions. A similar evaluation can be made between MS3 and MS4. Issues still remain regarding the differential influence of ceramics on slag chemistry and require that results be treated with caution. Nonetheless, all experimental samples are included for information.

Figure 14 shows the projection of slag specimens into the $FeO–SiO_2–Al_2O_3$ phase diagram. Group modes that approach the point labelled Optimum 1 are more depleted of FeO while those that approach Optimum 2 are richer in FeO. A comparison of the MIS6 and MS2 slag distributions suggest that the former may be leaner in FeO, but with substantial overlap. A comparison of MS3 and MS4 slag also fails to reveal any clear differences. The same results are obtained by comparing RII values (Fig. 15).

Mass balance calculations produce a very different picture, however (Table 9). Considered on an ordinal scale, MIS6 shows the greatest reduction efficiency followed by MS3, MS1, MS2 and MS4, respectively. The experimental yield results indicate a reduction efficiency order with MS1 as the most efficient followed by MS3, MS2 and MS4. The mass balances therefore create a reasonable, if not exact, correspondence to the experimental observations. Similarly, the placement of the MIS6 yield calculation aligns with the hypothesised high level of reduction efficiency based on slag microstructure (i.e. low concentrations of free iron oxides).

Discussion

The experimental smelts detailed in Humphris et al. (n.d.a, b) and whose residues are investigated here, failed to yield much iron or produce more than one flow of tap slag that resembles that found in the archaeology of MIS6. Analysis of the materials that were produced during the experiments, however, provides some new insights into bloomery smelting at Meroe during the Late and Post-Meroitic period. Most importantly, microstructural investigations of potential iron ore found within the archaeological furnace fill and those used in the experiments indicates the exploitation of an oolitic ore source, in line with suggestions by Abdu and Gordon (2004) and the single analysis published by Wainwright (1945). It is also clear that the ore used at MIS6 was not obtained in the iron-rich hills just east of Meroe as sometimes suggested (Tylecote 1982; Rehren 2001).. This is noted both in the structure of the ooids and in their chemistry. Identifying the true source of the ore remains an important challenge, one that could further benefit from the analysis of trace elements (especially the rare earth elements; see Leroy et al. 2012). This provides a potential avenue of future research.

The microstructure and chemistry of the archaeological and experimental TC are consistent with Tylecote's (1982) hypothesised use of local sand and Nile clay by Meroitic smelters. The chemical analyses also indicate a greater uniformity in TC preparation by past tuyère and furnace makers than was achieved for the experiments (see also Ting and Humphris 2017). The presence of slag as temper in these ceramics is noteworthy, though it is unclear whether or not its presence suggests intentional or incidental inclusion. On one hand, a crushed slag temper could pass on beneficial properties to the ceramic paste that increases its workability or industrial lifespan. On the other hand, the presence of crushed slag could be an accident of the spatial organisation of TC production and its proximity to ironmaking workshops. Of practical note, the sharp edges of crushed slag would be difficult to handle while fabricating the TCs. An investigation of sand constituents at different locations at Meroe may help resolve the issue and illuminate new details related to the production economy.

Analysis of the experimental and archaeological slag shows few similarities. Each experiment produced slag with a diverse range of microstructures that indicates inconsistent control over furnace redox conditions. This is a consequence

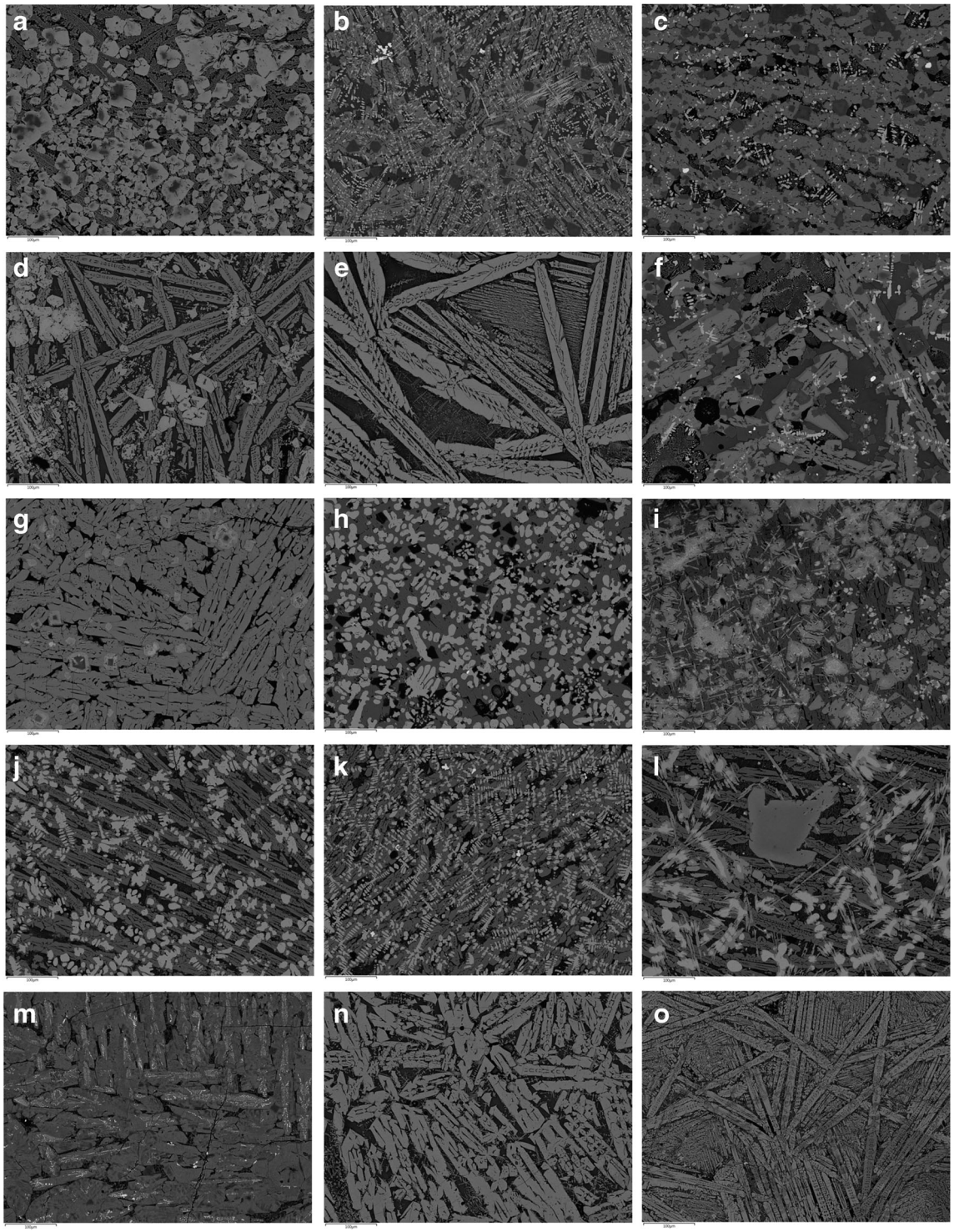

Fig. 11 BSE images of select slag specimens derived from the Meroe smelting experiments and the MIS6 furnace fill. The first four rows of images represent common slag microstructures from individual experiments, arranged in order from top to bottom. The bottom row represents the dominant slag microstructures observed in the archaeological furnace slag. **a** MS1-1-S_Area b; **b** MS1-2-S_Area d; **c** MS1-4-S_Area e; **d** MS2-12-S_area e; **e** MS2-13-S_area b; **f** MS2-15-S_area b; **g** MS3-3-S_area c; **h** MS3-4-S_area d; **i** MS3–7-S_area e; **j** MS4-2-S_area d; **k** MS4-3-S_area b; **l** MS4-6-S_area c; **m** MIS6-FW224-9-S_area b; **n** MIS6-FW224–11-S_area b; **o** MIS6-FW224-15-S_area a. See Charlton and Humphris (2017) for all SEM images collected in this study

of both poor air supply design and a variable draft (Humphris et al. n.d.a, b). Nonetheless, some MS2 slags do show the lean fayalite and glass microstructures observed in the MIS6 slags. This suggests that similar conditions were approached

Table 7 Chemical summary of experimental and archaeological slag for element concentrations greater than or equal to 0.1 wt. %

Context	wt.%	Na	Mg	Al	Si	P	K	Ca	Ti	Mn	Fe	Co	Zr	Ba
MIS6-FW224 (smelting (n = 8))	ȳ	0.20	0.23	4.42	14.00	0.52	0.21	1.36	0.73	2.06	40.58	0.19	0.13	0.28
	s	0.07	0.02	0.41	1.58	0.05	0.07	0.58	0.05	0.21	3.74	0.04	0.04	0.03
MS1 (smelting (n = 3))	ȳ	0.39	0.24	4.99	10.02	0.89	1.12	2.24	0.31	1.28	47.55	0.23	0.10	0.17
	s	0.08	0.03	0.46	0.95	0.06	0.24	0.52	0.05	0.10	3.25	0.02	0.04	0.04
MS2 (smelting (n = 2))	ȳ	0.18	0.15	4.98	13.65	0.39	0.30	1.19	0.34	0.98	45.19	0.23	0.04	0.15
	s	0.02	0.00	0.47	1.21	0.04	0.06	0.14	0.05	0.04	2.99	0.02	0.04	0.02
MS3 (smelting (n = 5))	ȳ	0.15	0.11	3.90	8.40	0.39	0.20	0.81	0.24	1.08	55.72	0.28	0.07	0.15
	s	0.03	0.02	0.28	2.15	0.07	0.09	0.22	0.02	0.15	3.16	0.03	0.04	0.02
MS4 (smelting (n = 5))	ȳ	0.23	0.29	3.90	9.45	0.68	0.99	2.15	0.21	0.59	51.36	0.24	0.10	0.04
	s	0.04	0.01	0.69	1.26	0.10	0.27	0.47	0.02	0.02	3.57	0.03	0.03	0.02
MIS6-FW262 (smithing (n = 2))	ȳ	0.30	0.27	1.94	8.22	0.25	0.30	0.86	0.25	0.74	50.52	0.25	0.06	0.08
	s	0.24	0.23	2.06	9.74	0.12	0.39	0.86	0.26	0.46	18.11	0.27	0.05	0.05

Means and standard deviations for specified chemical groups are calculated from normalized raw data found in Charlton and Humphris (2017)

in certain areas of the furnace for at least a brief time. What sets this experiment apart from the other three is the use of a leaner ore (similar in Fe concentrations to that sampled from MIS6) and a higher rate of air supplied over a longer period of time. This supports a model of Late–Post-Meroitic bloomery smelting that involved consistent redox conditions across the furnace plan and high volumes of air supplied during key stages of the smelt, if not its entirety.

The slag sample obtained from each experimental context could be discriminated by its chemistry. Differences in ore account for most of the differences, though variation in furnace operation accounts for dissimilarities in fuel ash and TC influences. None, however, used ores that matched those of found in the MIS6 furnace fill.

It is worth noting that only MS4 included the addition of a furnace lining similar to that found on site. Tylecote's (1982) investigation revealed this lining to be comprised of large sand grains fused together with vitrified clay and slag. Silica, the major constituent in the sand at Meroe, is refractory and the large grains would serve to lessen reactivity. Such a lining would be less prone to thermochemical attack and would have a reduced influence on slag chemistry. This does not preclude, however, the potential influence of melting tuyères or unlined portions of the furnace walls. The MS4 lining did not have time to cure prior to commencement of the smelt and accounts, at least in part, for the experiment's performance. Nonetheless, it is not surprising that mass balances indicate less ceramic input in the archaeological slag produced in a lined furnace compared with that from the experiments.

The ceramic contribution tends to increase the average concentrations of Al and Si in the slag, thereby diluting the concentration of elements more common in the ores, especially Fe. This influence can impact other analyses seeking to identify differences in redox conditions. This is observed in both the ternary and RII models, rendering them ineffective as proxy measures of relative redox conditions. Calculating the mass balance provides a means of estimating ceramic and ore inputs as well as Fe yields. The accuracy of that estimate,

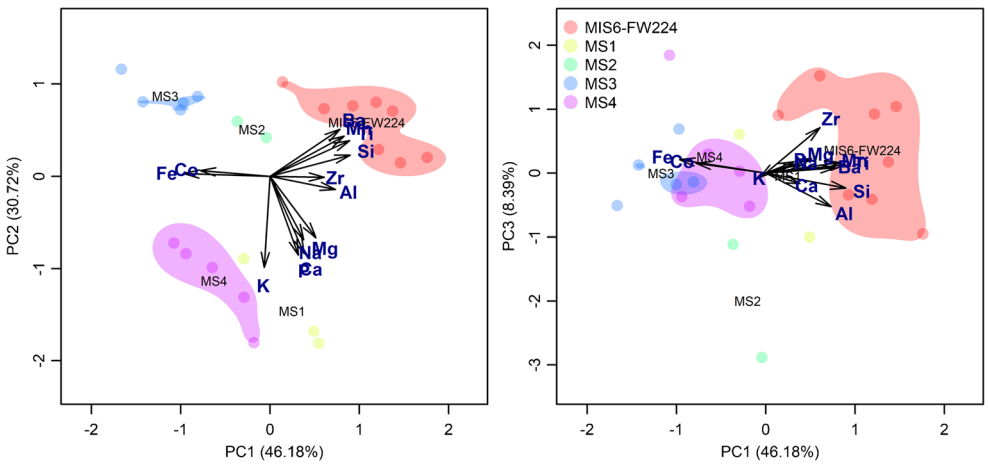

Fig. 12 PCA biplots of experimental and archaeological slag chemistry. Outlying fuel ash and ceramic-rich specimens were identified and removed in order to enhance comparability between smelts. Clustering is attributed to resource utilization, furnace temperature and redox conditions. Slag context names are plotted at the centres of their projected distributions

Table 8 Contingency table for modelling resource-delimited constraints defined by positive oxide correlations

	Na	Mg	Al	Si	P	K	Ca	Ti	Mn	Fe	Co	Zr	Ba
Na		FA	TC	TC	FA	FA-TC	TC	TC	TC			TC	TC
Mg	FA		O	O	O-FA	FA	O-FA	O	O	O	O	O	O
Al	TC	O		TC	O	TC	O	O-TC	O	O	O	TC	O-TC
Si	TC	O	TC		O	TC	O	TC	O	O	O	TC	O-TC
P	FA	O-FA	O	O		FA	O-FA	O	O	O	O	O	O
K	FA-TC	FA	TC	TC	FA		FA	TC		TC	O	O-TC	TC
Ca	FA	O-FA	O	O	O-FA	FA		O	O	O	O	O	O
Ti	TC	O	O-TC	TC	O	TC	O		O	O	O	O-TC	O-TC
Mn	TC	O	O	O	O		O	O		O	O	O	O
Fe		O	O	O	O	TC	O	O	O		O	O	O-TC
Co		O	O	O	O	O	O	O	O	O		O	O
Zr	TC	O	TC	TC	O	O-TC	O	O-TC	O	O	O		O-TC
Ba	TC	O	O-TC	O-TC	O	TC	O	O-TC	O	O	O	O-TC	

O, ore; FA, fuel ash; TC, technical ceramic

however, depends on chemical measures that share common sources of error. While the analysis of glass basalt CRMs is useful for knowing that the SEM-EDS produces high-quality results under ideal conditions, it does not account for uncertainties introduced by varying levels of sample heterogeneity and porosity. This limitation becomes greater when considering the ore and ceramic analyses. Comparisons between the samples of similar structure and chemistry will share similar patterns of error, but comparisons between ore, ceramic and slag (as used in the mass balance calculations), becomes problematic. The results of such any analysis must be regarded with caution and considered ordinal scale at best.

A second complication affects the ternary model, RII and mass balance measures. Each considers the identified smelting slag and not the large volume of unreacted and partly reacted ore that was also produced during the experiments. The models assume that all of the ore reacts completely to form metal and slag. This assumption holds greater validity for archaeological slag heaps where it is typical to find negligible amounts of intermediate ore-slag products and is indicative of a mature smelting process. The intermediate products were, however, non-negligible in the experiments discussed here. Thus, all the mass balance calculations over-estimate the amount of iron produced per smelt and may account for the erroneous ordering of MS1 and MS3 in terms of yield.

Conclusions

The experimental iron smelts at Meroe, Sudan and the questions that arose during and after the campaign succeeded in shedding light on Late and Post-Meroitic ironmaking practices despite their failures to produce large quantities of iron or slag of appropriate character. Ore investigations revealed that an oolitic ironstone was exploited that was not, or at least is no longer, available in the immediate site vicinity. Resources used for the production of TC are consistent with the hypothesis of local exploitation of sand and Nile clay. The similarity of slag

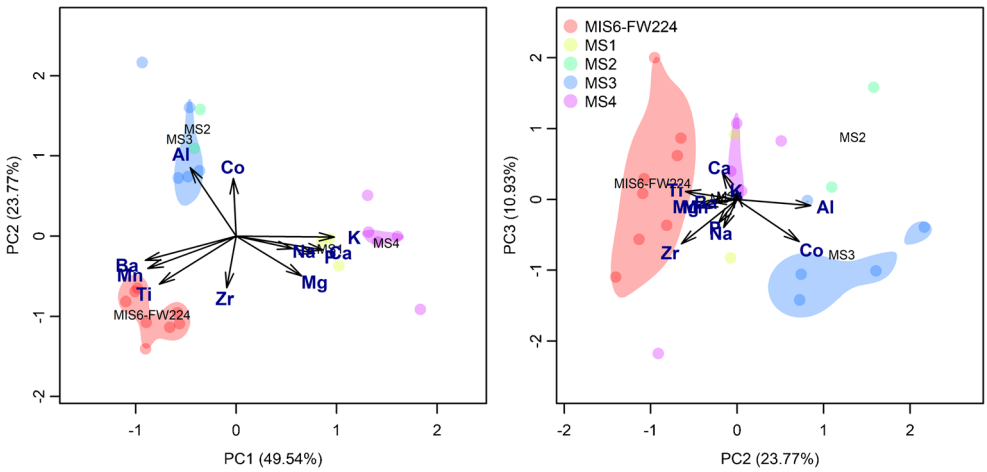

Fig. 13 PCA biplots of experimental and archaeological slag chemistry. Fe and Si are removed from consideration to better emphasize resource differences. Specimens include slag collected from the Meroe bloomery experiments as well as slag excavated from the MIS6 furnace workshop floor. Slag context names are plotted at the centres of their projected distributions

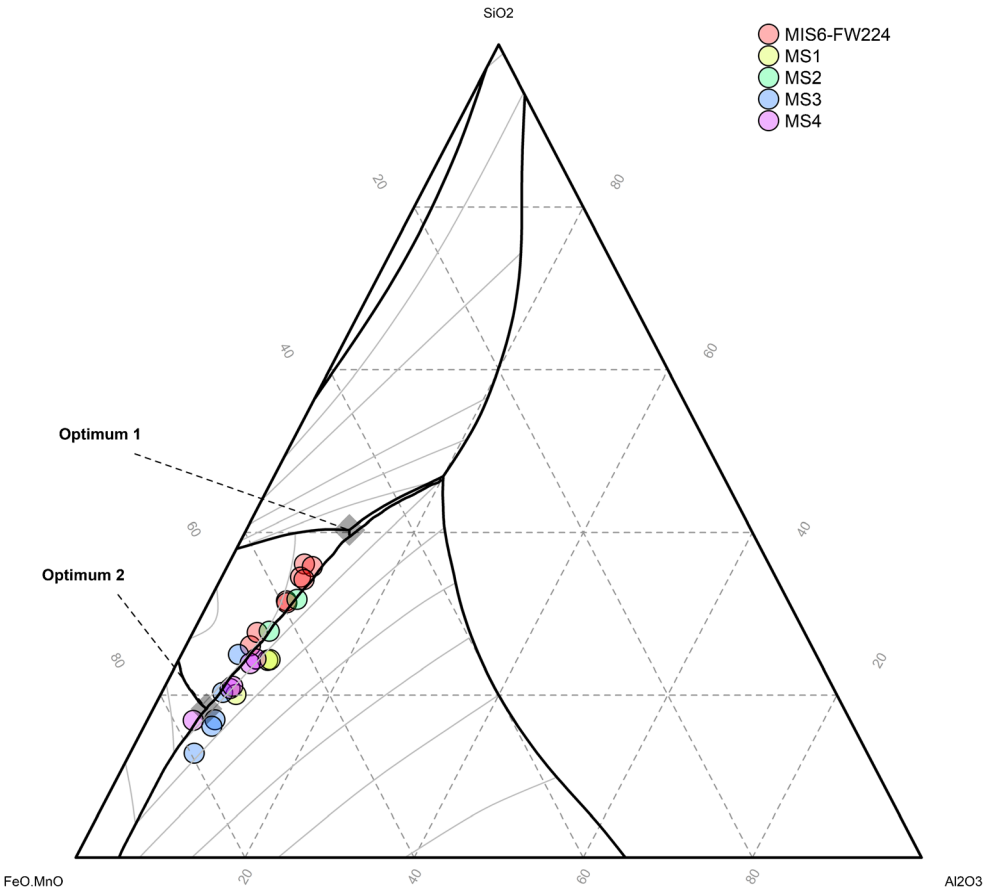

Fig. 14 MIS6 and experimental slag plotted in the FeO–SiO_2–Al_2O_3 ternary system. MnO is combined with FeO because of their similar chemical behaviour. Isotherms are not included as they are modelled for ideal equilibrium conditions that the actual slag do not represent

microstructures between MS2 and MIS6 provides evidence that Late and Post-Meroitic iron producers created more consistent redox environments within their furnaces. This has implications for both the design of the air supply system and its operation. Finally, the mass balances, while limited, are consistent with the hypothesis that a specially prepared furnace lining is an essential part of Meroitic smelting practice and necessary for producing slag with similar properties to those found within the archaeometallurgical record of the site.

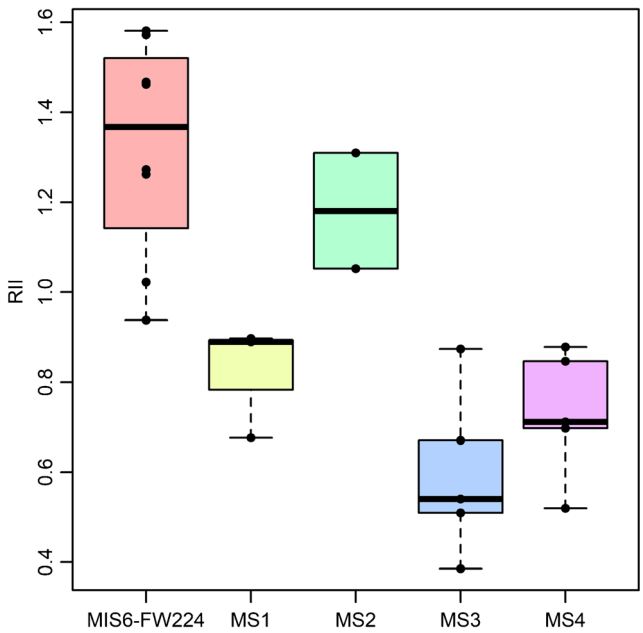

Fig. 15 Boxplot of MIS6 and experimental slag RII values

The strength of the insights derived from this investigation must, of course, be tempered by the fact that the archaeological residues reflect what was probably the last smelt conducted in the MIS6 furnace. It is unlikely to be representative of the some 300 years of smelting practices that may have contributed to the slag heap's formation. Smelting practices and ore sources may have, and probably did, change over time.

Table 9 Mass balance results for Meroe bloomery experiments and MIS6 furnace fill

Context	% ore	% clay	% yield	Fe production/100 units slag
MIS6	95.5	4.5	54.9	61.3
MS1	85.5	14.5	44.9	43.2
MS2	76.5	23.5	23.4	17.2
MS3	89.5	10.5	45.9	55.2
MS4	79.0	21	17.0	10.3

Values derived following the method described in Crew (2000). Unknown data quality differences for ore, clay and slag analyses force all estimates to be treated as ordinal-scale values

The findings of this small scale experimental study and the questions they raise have had immediate impacts on the direction of research. Preliminary ore results led to a new search for a potential ore source and the identification of a previously unrecorded Meroitic mining area in hills about 9 km to the northeast of the Royal City. Research on the character of the ironstone samples extracted from subsequent archaeological investigation of this mining area is ongoing. More intensive petrographic investigations are also providing a better model of ancient technical ceramic ecology (Ting and Humphris 2017). Evidence for diachronic variability, along with the considerations above, is being explored in ongoing field and laboratory investigations. A critical assessment of the experimental design has also led to a new experimental campaign in autumn 2017. Perhaps the most important impact, however, is in recognising the critical role played by experimental archaeology in exploring, challenging and extending models of past human behaviour.

Acknowledgements Permission for the research to be carried out at Meroe is granted by the National Corporation for Antiquities and Museums in Sudan, and for their assistance and continual support, we are sincerely thankful. Fareed Alshishani, Loic Boscher and Tom Birch selected and prepared samples for microscopy with support from Philip Connelly. Carmen Ting offered insights on ceramic selection and Robert Bussert made valuable comments about the local Geology of Meroe. Frank Stremke prepared the project map. Special thanks go to smelters Jake Keen and Lee Sauder for conducting the experiments and Suleiman Awad Suleiman, Thomas Scheibner and Saskia Büchner for constant and multifaceted assistance throughout the project. Comments made by two anonymous reviewers have helped us clarify many key points. Finally, the field team working in Sudan and the local communities around Meroe are thanked for their patience and support.

Funding information A number of organisations provide collaborations and funding through with various aspects of this research have been greatly assisted. These include the Qatar-Sudan Archaeology Project (grant 037), UCL Qatar, the University of Khartoum, and the British Institute in Eastern Africa. Michael Charlton's participation and research was supported by a Marie Curie International Incoming Fellowship (PIIF-GA-2013-624448) within the 7th European Community Framework Programme as part of the IRONWORKS project.

References

Abdu B, Gordon R (2004) Iron artifacts from the land of Kush. J Archaeol Sci 31(7):979–998. https://doi.org/10.1016/j.jas.2003.12.011

Baxter MJ, Freestone IC (2003) Log-ratio analysis in archaeometry glass compositional data. Archaeometry 48:511–531

Charlton M, Humphris J (2017) Exploring ironmaking practice at Meroe, Sudan—images, data, and analytical scripts,V1. Harvard Dataverse. https://doi.org/10.7910/DVN/HQZOOB

Charlton MF, Crew P, Rehren T, Shennan SJ (2010) Explaining the evolution of ironmaking recipes—an example from northwest Wales. J Anthropol Archaeol 29(3):352–367. https://doi.org/10.1016/j.jaa.2010.05.001

Charlton MF, Shennan SJ, Rehren T, Crew P (2013) Evolutionary analysis of ironmaking slag. In: Humphris J, Rehren T (eds) The world of iron. Archetype Publications Ltd, London, pp 288–395

Crew P (2000) The influence of clay and charcoal ash on bloomery slags. In: Tizzoni C, Tizzoni M (eds) Iron in the Alps: deposits, mines and metallurgy from antiquity to the XVI century. Proceedings of the conference, Bienno, pp 38–48

Crew P (2013) Twenty-five years of bloomery experiments: perspectives and prospects. In: Dungworth D, Doonan RCP (eds) Accidental and experimental archaeometallurgy. Historical Metallurgy Society, London, pp 25–50

Crew P, Charlton MF, Dillmann P, et al (2012) Cast iron from a bloomery furnace. In: Hošek J, Cleere H, Mihok L (eds) The archaeometallurgy of Iron: recent developments in archaeological and scientific research. Praha, pp 239–262

Humphris J (n.d.) Iron and Kush. In: Oxford handbook of Nubian archaeology. Oxford University Press, Oxford

Humphris J, Carey C (2016) New methods for investigating slag heaps: integrating geoprospection, excavation and quantitative methods at Meroe, Sudan. J Archaeol Sci 70:132–144. https://doi.org/10.1016/j.jas.2016.04.022

Humphris J, Rehren T (2014) Iron production and the Kingdom of Kush: an introduction to UCL Qatar's research in Sudan. In: Lohwasser A, Wolf P (eds) Ein Forscheleben zwischen den Welten. Sonderheft, Berlin, pp 177–190

Humphris J, Scheibner T (2017) A new radiocarbon chronology for ancient iron production in the Meroe region of Sudan. African Archaeol Rev 34(3):377–413. https://doi.org/10.1007/s10437-017-9267-x

Humphris J, Bradshaw R, Emberling G (n.d.a) Archaeologists and communities in Sudan's Nile Valley. In: Emberling G, Williams B (eds) Oxford handbook of ancient Nubia. Oxford University Press, Oxford

Humphris J, Charlton MF, Keen J et al (n.d.b) Iron smelting in Sudan: experimental archaeology at the Royal City of Meroe. J F Archaeol

Leroy S, Cohen SX, Verna C, Gratuze B, Téreygeol F, Fluzin P, Bertrand L, Dillmann P (2012) The medieval iron market in Ariège (France). Multidisciplinary analytical approach and multivariate analyses. J Archaeol Sci 39(4):1080–1093. https://doi.org/10.1016/j.jas.2011.11.025

Plumlee G (1998a) Basalt, Columbia River, BCR-2. U.S. Geological Survey, Denver

Plumlee G (1998b) Basalt, Hawaiian volcanic observatory, BHVO-2. U.S. Geological Survey, Denver

R Core Team (2017) R: a language and environment for statistical computing. R Foundation for Statistical Computing, Vienna. (https://www.r-project.org/)

Rehren T (2001) Meroe, iron and Africa. MittSAG 12:102–109

Rehren T, Charlton MF, Chirikure S et al (2007) Decisions set in slag—the human factor in African iron smelting. In: La Niece S, Hook D, Craddock P (eds) Metals and mines: studies in archaeometallurgy. Archetype Publications Ltd, London, pp 211–218

Shinnie PL, Kense FJ (1982) Meroitic iron working. Meroitica 6:17–28

Smith DB (1998) Icelandic basalt, BIR-1

Ting C, Humphris J (2017) The technology and craft organisation of Kushite technical ceramic production at Meroe and Hamadab, Sudan. J Archaeol Sci Reports 16:34–43. https://doi.org/10.1016/j.jasrep.2017.09.017

Török L (2015) The periods of Kushite history, from the tenth century BC to the AD fourth century. Ízisz Foundation, Budapest

Trigger BG (1969) The myth of Meroe and the African Iron Age. Afr Hist Stud 2:23–50

Tylecote RF (1982) Metal working at Meroe, Sudan. Meroitica 6:29–42

Tylecote RF, Austin JN, Wraith AE (1971) The mechanism of the bloomery process in shaft furnaces. J Iron Steel Inst 209:342–363

Wainwright GA (1945) Iron in the Napatan and Meroitic ages. Sudan Notes Rec 26:5–36

Welsby DA (1996) The Kingdom of Kush: the Napatan and Meroitic empires. Markus Wiener Publishers, Princeton